minerals

MDPI

Article

Cesium Sorption and Desorption on Glauconite, Bentonite, Zeolite and Diatomite

Petr Belousov [1,*], Anna Semenkova [1,2], Tolganay Egorova [2], Anna Romanchuk [2], Sergey Zakusin [1,3], Olga Dorzhieva [1,4], Ekaterina Tyupina [5,6], Yulia Izosimova [7], Inna Tolpeshta [7], Michail Chernov[3] and Victoria Krupskaya [1,3,8,]

1 Institute of Geology of Ore Deposits, Petrography, Mineralogy and Geochemistry, Russian Academy of Science (IGEM RAS), 119017 Moscow, Russia; annamik88@rambler.ru (A.S.); zakusinsergey@gmail.com (S.Z.); dorzhievaov@gmail.com (O.D.); krupskaya@ruclay.com (V.K.)
2 Department of Geology, Lomonosov Moscow State University (MSU), 119899 Moscow, Russia; tolganay@mail.ru (T.E.); romanchuk.anna@gmail.com (A.R.)
3 Department of Chemistry, Lomonosov Moscow State University (MSU), 119899 Moscow, Russia; chernov@geol.msu.ru (M.C.)
4 Geological Institute, Russian Academy of Science (GIN RAS), 119017 Moscow, Russia
5 Department of High Energy Chemistry and Radioecology, D. Mendeleev University of Chemical Technology of Russia (MUCTR), 125480 Moscow, Russia; tk1972@mail.ru
6 Department of Closed Nuclear Fuel Cycle Technology, National Research Nuclear University, 115409 Moscow, Russia
7 Department of Soil Science, Lomonosov Moscow State University (MSU), 119899 Moscow, Russia; izosimova.julya@yandex.ru (Y.I.); sokolt651@mail.ru (I.T.)
8 The Nuclear Safety Institute, Russian Academy of Science (IBRAE RAS), 115191 Moscow, Russia
* Correspondence: e-mail: pitbl@mail.ru; Tel.: +7-926-187-39-47

Received: 29 July 2019; Accepted: 10 October 2019; Published: 11 October 2019

Abstract: This study is devoted to studying the sorption of ^{137}Cs on mineral sorbents at a wide pH range, from 2 to 10, as well as to studying sorption mechanisms. In order to obtain the most reliable sorption characteristics, samples of high purity were examined as sorbents: bentonite, glauconite, zeolite, and diatomite. A detailed description of their mineral composition, cation exchange capacity and specific surface of sorbents is given. XRD, XRF, FTIR, SEM, and BET adsorption methods were used for assaying. The sorption and desorption values were identified for each sorbent. As a result of the conducted research, it can be concluded that ^{137}Cs sorption mainly occurs through the exchange reaction on zeolite, glauconite and bentonite. The highest cesium Kd was observed on zeolite due to its high CEC and amounted to 4.05 mg/L at pH 7. The higher sorption capacity of glauconite in comparison with bentonite is primarily due to the high layer charge which is mainly localized in tetrahedral sheets, and to the existence of highly selective sorption sites (frayed edge sites) on the glauconite surface. Diatomite showed the lowest sorption capacity provided by the presence of a small quantity of smectite and kaolinite in its composition. The values of desorption increase in the following order: zeolite < bentonite ~ diatomite < glauconite.

Keywords: cesium; sorption; desorption; mineral sorbents; bentonite; montmorillonite; glauconite; zeolite; diatomite

1. Introduction

The term "natural sorbent" is valid for rocks from a wide range of mineral deposits. They differ in sorption capacity and mechanism, as well as in selectivity to pollutants [1].

There are two main groups of sorbents according to the filtration properties of the materials based on them: permeable and non-permeable sorbents. The non-permeable sorbents include

bentonites, which were proposed as barrier materials for use in underground repositories for the disposal of high-level radioactive wastes. Their features are low hydraulic conductivity after swelling in a confined space, high cation exchange, and adsorption capacity [2,3]

In addition to the safety assurance of high-level wastes to be buried in underground repositories, the safety of other nuclear legacy waste objects is required, including: the isolation of intermediate and low-level wastes in near surface disposal facilities, the decommissioning of liquid radioactive waste storage facilities and complex structural objects, and the remediation of contaminated areas. A common problem of the nuclear legacy objects is the vicinity of hydrographic systems, which requires waterproofing barriers and the construction of permeable barriers for the efficient radionuclide sorption in wastewater drainage systems. Widely used, low-cost natural sorbents can be utilized for this purpose.

In this article, argillaceous (bentonite and glauconite) as well as non-argillaceous (zeolite and diatomite) sorbents have been studied. They have different mineral composition, sorption and filtration properties. Smectite minerals, predominantly montmorillonite, are the basic components of bentonite. They are a class of layered aluminosilicates which consist of two tetrahedral sheets and one octahedral sheet in between forming together a 2:1 layer. Due to isomorphic substitutions in octahedral and tetrahedral sheets, the whole layer acquires a negative charge, which is compensated by interlayer cations thus resulting in the high sorption properties typical of smectite minerals [4]. Glauconites belong to the interlayer-deficient mica group, they are a kind of Fe-rich type of illite. Interlayer-deficient micas have a layer structure similar to smectite (2:1), however, their characteristic feature is the presence of a strongly bonded potassium cation in the interlayer space and a high layer charge.

Zeolites, also known as molecular sieves for their specific structure and properties, are hydrated framework aluminosilicates (tectosilicates) with intracrystalline channels and cavities. Due to the isomorphous substitution of Al for Si, the negative charge is formed in the channels, which requires compensation by cations causing a high selectivity for zeolites to a number of substances including radionuclides. Diatomites are siliceous rocks consisting of remnants of diatomaceous algae possessing high specific surface area due to their very fine average particle size and therefore micro- and macroporosity [5].

The usage of natural zeolites, such as mordenite, erionite and chabazite, for radioactive waste decontamination has been suggested by a number of authors [6–8]. Diatomite has been considered as a filter for the elimination of ^{137}Cs and some other metals from nuclear reactor cooling water [9]. Natural and modified forms of diatomite have been used for the removal of organic compounds, heavy metals and radionuclides from liquid waste [5].

The novelity of this research is to study the value of sorption of cesium on natural sorbents with different mineral composition and physicochemical properties at a wide pH range (2–10) so that the results may be used in a wide range of natural conditions. Since the most natural sorbents contain significant amounts of impurities with high sorption capacity (especially clays), in the present work we used purified (neat) minerals from industrial deposits with a maximum quantity of the target component, which made it possible to establish more accurate sorption characteristics.

The use of natural sorbents without preliminary detailed mineralogical studies can lead to incorrect interpretation of the results. Even a small admixture of clay minerals which is especially characteristic of diatomite and zeolite, can significantly distort the sorption values. In order to understand the mechanisms of sorption on each sorbent, additional studies of the mineral and their structural features were carried out, including infrared spectroscopy, electron microscopy, determination of surface characteristics and cation exchange capacity. In order to study the ability of sorbents to retain cesium, a desorption experiment was conducted. The data obtained helped not only to establish the desorption value, but also to understand the mechanisms of cesium binding in natural sorbents in more detail. This approach makes it possible to determine the minerals responsible for binding particular radionuclides, which in turn would allow for the proposal of a filtration mixture composition suitable for the specific radioactive contaminants' composition.

2. Materials and Methods

2.1. Mineral Sorbent Sources

In order to study sorption mechanisms, sorbents with high contents of target components were chosen. The chosen argillaceous minerals were: enriched bentonite (10th Khutor deposit, Russia) and enriched glauconite (Karinskoye deposit, Russia). The non-argillaceous sorbents were: zeolite (Sokernitskoye deposit, Ukraine), and diatomite BiaFa (Munsingen, Germany).

The most difficult challenge in analyzing the physicochemical properties of different sorbents is the lack of reliable information on their mineral composition or a relatively high content of impurities, especially those of clay minerals, which can significantly alter the properties of the sorbents. To obtain the correct information about sorption on the selected sorbents, enriched industrial products (diatomite and zeolite) or laboratory-enriched materials (bentonite and glauconite) were selected.

The industrial diatomite sample contained, as shown below, a certain amount of clay minerals, which is typical for the majority of industrial and natural samples of diatomite. However, since the diatomite and clay particles or their aggregates have similar specific gravity and size, it was not possible to enrich this material. Thus, the "purest" natural product offered by the company BiaFa was chosen.

It was also not possible to enrich the natural zeolite samples from the deposits of the Russian Federation (Badinskoe, Shivertuyskoe, Talan-Gozagorskoe, Holinskoe deposits), the content of zeolite in the examined samples varied from 40% to 72%. Thus, in the present research, it was decided to use the material with the highest content of the desired component, this being the sample from the Sokernitskoye deposit.

The industrial sample from the Karinskoye glauconite deposit was additionally enriched using an electromagnetic separator (50 A, 30 mv) (RPPP, Moscow, USSR) to obtain a most concentrated fraction of the examined component.

The source minerals of bentonite clays are smectites (mainly montmorillonite, sometimes with admixtures of beidellite, nontronite or saponite). To obtain an enriched sample of bentonite, i.e., a material with maximum smectite content, a 0.5 μm fraction was separated by centrifuge OS-6MS (Dastan, Bishkek, Kyrgyzstan) at a speed of 1200 rpm for 10 min.

2.2. General Characterization of the Mineral Sorbents

Powder X-Ray diffraction (XRD), X-ray fluorescence (XRF), infra-red (FTIR) spectroscopy, and scanning electron microscopy (SEM) methods were used to characterize the sorbents. Evaluation of specific surface area (S_{BET}) and various methods for determining the cation exchange capacity (CEC) were used for the analysis of sorption capacity. X-ray diffraction patterns were obtained with an X-ray diffractometer Ultima-IV (Rigaku, Tokyo, Japan) acquired with the funding of Moscow State University Development Program (Cu-K_α radiation, semiconductor 1D detector D/Tex-Ultra, scan range 3–65°2θ, scan speed 3°2θ/min and step—0.02°2θ). Non-textured powder specimens were prepared by sieving the sample powder into a sample holder and cutting the excess material with a razor. The mineral composition was analyzed according to the method of [10], the quantitative composition was estimated using the Rietveld method [11] with the Profex software (Version 3.14.3, Nicola Doeblin, Solothurn, Switzerland, 2019)[12].

Chemical analysis was performed using the X-ray fluorescence method in accordance with standard procedure using the spectrometer Axios mAX (PANalytical, Almelo, The Netherlands) at IGEM RAS (Moscow). Samples were dried at 110 °C and prepared by fusion with lithium borate at 1200 °C. The iron content was determined only as the total Fe_2O_3, regardless of the actual valence state of the Fe.

IR absorption spectra were obtained using a Bruker FTIR spectrometer Vertex 80v (GIN RAS) (Billerica, MA, USA) equipped with a DTGS detector and a KBr beam-splitter. The spectra recordings were performed in a vacuum in the 4000–400 cm^{-1} wavelength range with 256 scans for each sample and a resolution of 4 cm^{-1}. Specimens were prepared as pressed KBr-pellets: 0.5 mg of the sample was dispersed in 200 mg of KBr; this mixture was placed in a 13 mm pellet dish and pressed in vacuum

for 1 h. The KBr pellet was then placed into a glass desiccant box with $CaCl_2$ and heated in a furnace at 105 °C for at least 20 h. Baseline correction was made with the OPUS soft (version 7.1, Brucer, Billerica, MA, USA) in interactive mode using straight line and one iteration.

The microstructure of the sorbents was studied with a scanning electron microscope (SEM) LEO1450VP (Carl Zeiss, Oberkochen, Germany) acquired with the funding of the Moscow State University Development Program. Samples for SEM were prepared in the form of individual particles and aggregates. A sample in powder form was deposited on a double-sided electrically conductive adhesive tape. Then the excess sample particles were removed with compressed air. As a result, a monolayer of individual particles and aggregates on an adhesive tape was obtained. The studied surface was coated with a thin gold film, 5–10 nm thick, under vacuum. A conductive coating is required to avoid the electrical charging of the sample during analysis.

Evaluation of the specific surface area was carried out using a Quadrasorb SI/Kr analyzer (Quantachrome Instruments, Boynton Beach, FL, USA). Adsorption was performed at the temperature of liquid nitrogen (77.35 K). Nitrogen with a purity of 99.999% served as an adsorbate. Helium grade 6.0 (99.9999%) was used for the volume calibration of the measuring cells. The calculation was carried out by the BET multiple-point isotherm in the range of P/P0 from 0.05 to 0.30. Before measuring the surface characteristics, the samples were vacuum-pumped using the Flo-Vac Degasser installation, which is an integral part of the Quadrasorb SI/Kr analyzer and allows pumping of gases and water from the pore space in the temperature range of 15–400 °C and control of the pressure in the system (with the sample) in the range of 101.3 kPa–0.133 Pa. In our work, the pumping of the samples was carried out at 100 °C (temperature of dehydration) to a residual constant pressure in the system of 0.133 Pa. Using of a higher temperature can damage the structure of the aluminosilicates and, therefore, change the state of the pore space. The pumping time at this temperature was 4 h.

In view of the diversity of mineral sorbents, the cation exchange capacity (CEC) was determined by three methods: by the adsorption of methylene blue (MB), Mehlich's method (cation exchange in a 0.1 M solution of $BaCl_2$), and the use of an ammonium chloride solution.

Determination of the cation exchange capacity by MB sorption was carried out in accordance with international standards [13] and implicates titrating a clay suspension with MB solution to its excess in solution.

The method for determining the CEC by Mehlich [14] involves an exchange reaction with Ba^{2+} in a 0.1 M solution of $BaCl_2$ buffered with triethanolamine to a pH of 8.2. Concentrations of the exchanged Ca, Mg, Na and K in the solution were determined with an Agilent 5110 inductively-coupled plasma optical emission spectrometer (Agilent, Santa Clara, CA, USA).

The method for determining the CEC with an ammonium chloride solution is a standard technique for working with zeolites [15]. This method is based on cation exchange by NH_4^+, followed by the determining of the content of the exchanged Ca^{2+}, Mg^{2+}, Na^+, and K^+ in the solution by atomic absorption spectroscopy.

2.3. Sorption Experiments

^{137}Cs sorption was studied at concentration 10^{-6} M. The total concentration was obtained by adding the required quantity of stable CsCl solution to the ^{137}Cs tracer. Aliquots of CsCl and ^{137}Cs were added to 1 g/L clay suspensions in a 0.01M $NaClO_4$ solution. A concentration of 0.01 $NaClO_4$M was chosen to maintain a constant ionic strength in the solution. After adding the radionuclide, the pH was measured using a combined glass pH electrode (InLab Expert Pro, Mettler Toledo, Columbus, OH, USA) and adjusted by the addition of small amounts of diluted $HClO_4$ or NaOH solutions. The samples were mixed continuously using an end-over-end mixer. After 24 h (equilibrium time was taken from the paper [16]), the equilibrium pH was measured and 1 mL of each suspension was centrifuged at 40,000× g (Allegra 64R, Beckman Coulter, Brea, CA, USA) for 15 min to remove colloidal mineral particles, and the supernatant was collected and used for radioactivity measurements.

The concentration of ^{137}Cs was measured by liquid scintillation counting using a Quantulus-1220 (Perkin Elmer, Waltham, MA, USA) device.

The sorption value was calculated based on the difference between the radioactivity of the ^{137}Cs initially added to the suspension and the radioactivity remaining in the supernatant after equilibrium. The distribution coefficient (Kd), which quantifies the distribution of a dissolved element between the solution and the solid phases was calculated as follows:

$$Kd = \frac{\text{Atot} - \text{Asol}}{\text{Asol}} \times \frac{L}{S} \quad (1)$$

where Atot is the total activity added to the system, in Bq, Asol is the equilibrium activity in the liquid phase, in Bq, S is mass of the clay, in g, and L is the total volume of the suspension, in mL. Kd is one of the common units to represent sorption results [17–19].

Experiments to determine the reversibility of sorption were conducted after three months of equilibrating the samples with a solution of Cs, then desorption was carried out. For this, the $NaClO_4$ solution was completely replaced with 10 ml of model natural water ($NaHCO_3$—96.0 mg/L, $CaSO_42H_2O$—60.0 mg/L, $MgSO_4$—60.0 mg/L, KCl—4.0 mg/L [20]), and the samples were placed on a shaker. At predetermined time intervals, an aliquot was taken from the samples, it was centrifuged, and the content of desorbed cesium was measured.

3. Results and Discussion

3.1. Mineral Sorbents Characterization

The main obstacle in the study of sorption properties of natural sorbents, in most cases, is the contamination of the clay minerals, typically with illite and smectite. Due to the high sorption capacity of these components, a significant portion of a radionuclide can be sorbed by these impurities resulting in an incorrect interpretation of the results. In order to minimize the influence of clay admixtures on the sorption of cesium on natural sorbents, samples with a high content of the target component (more than 71%) were used. Chemical and mineral compositions are shown in Tables 1 and 2, respectively.

Table 1. Chemical composition of the examined samples, %.

Sample Name	LOI	Na_2O	MgO	Al_2O_3	SiO_2	K_2O	CaO	TiO_2	MnO	Fe_2O_3	P_2O_5	SO_3
Glauconite	9.94	0.07	3.75	7.61	50.52	6.94	0.59	0.12	0.016	19.72	0.21	<0.02
Bentonite	20.40	11.48	2.35	16.09	44.63	0.32	0.17	0.55	0.015	2.93	0.07	<0.02
Zeolite	8.56	1.48	0.65	13.14	68.62	3.35	2.38	0.16	0.041	1.11	0.02	<0.02
Diatomite	10.87	0.08	0.29	4.31	81.9	0.1	0.38	0.13	0.02	1.79	0.04	<0.02

Table 2. Mineral composition of the examined samples, %.

Mineral	Glauconite	Bentonite	Zeolite	Diatomite
Glauconite	99.6			
Opal				80.8
Clinoptilolite			71.8	
Smectite		96.8	1.4	9.9
Illite			8.4	
Kaolinite*				9.0
Quartz	0.4	2.4	15.0	0.3
Anatase		0.8		
Albite			3.4	
Total content	100	100	100	100

* Disordered kaolinite or probably halloysite or mixed-layer kaolinite-smectite.

XRD analysis revealed the composition of the glauconite sample: 99.6% glauconite mineral and 0.4% quartz as an impurity. A high iron content is typical for glauconite (Figure 1) and is isomorphically localized mainly in the octahedral sheet. Glauconite was identified by the series of basal (10.15 Å, 5.06 Å, 3.34 Å, 2.00 Å, etc.) and non-basal (4.54 Å, 2.59 Å, 2.41 Å, 1.51 Å, etc.) reflections. Another indirect indicator is a relatively high background level, as compared with the intensity of the main peaks, resulting from fluorescent radiation generated while analyzing the iron-rich samples using a copper anode. Quartz was identified by the relatively sharper part of the peaks at 3.34 Å and 4.27 Å, while the other peaks are less manifested due to the low content.

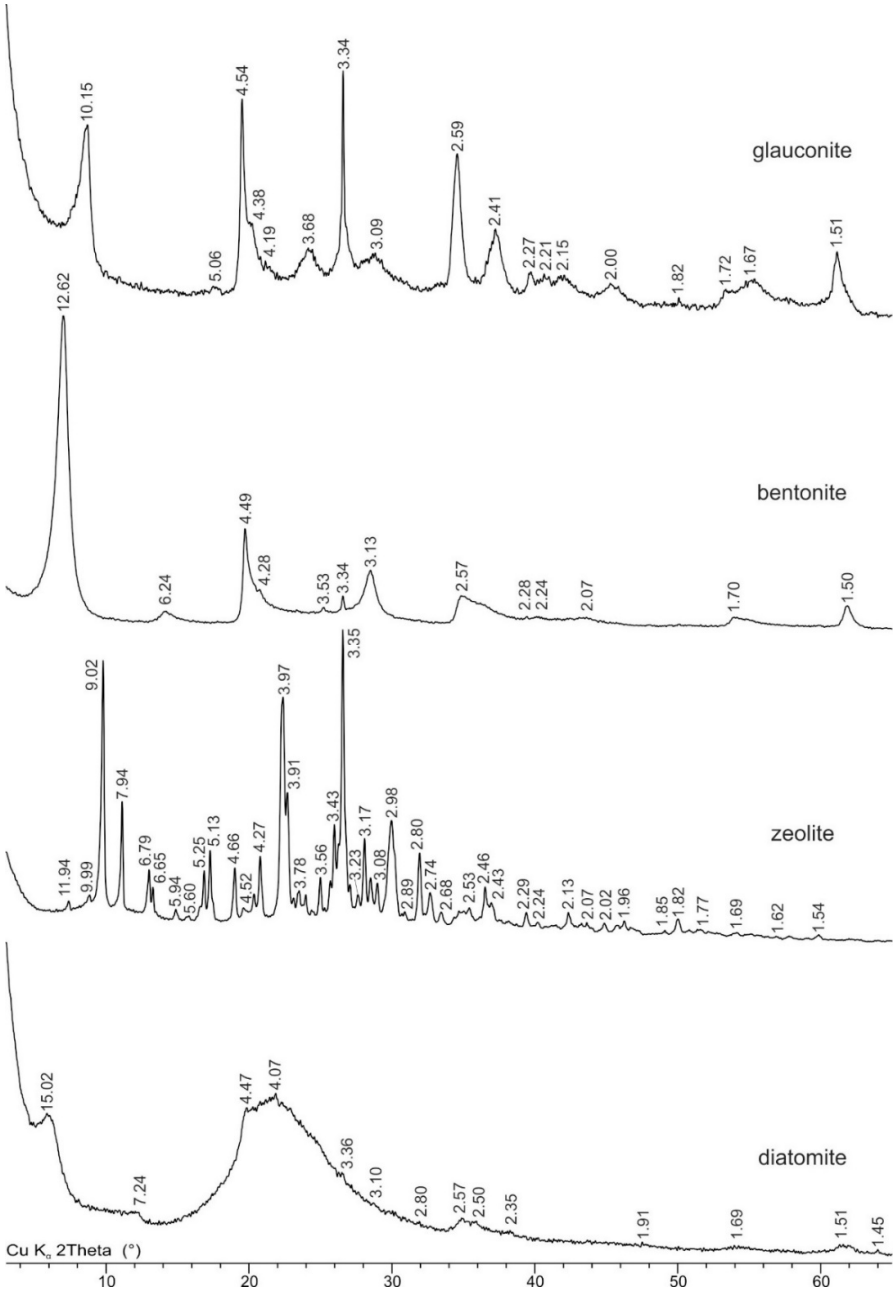

Figure 1. Powder X-Ray diffraction patterns of natural sorbents. D-spacings are given in angstroms.

The purified sample of bentonite from the 10-th Khutor deposits predominantly consisted of 96.8% Na-montmorillonite (Figure 1.). Impurities were represented by 2.4% of quartz and 0.8% of anatase. Montmorillonite was identified by a series of basal (12.62 Å, 6.24 Å, 3.13 Å and 2.07 Å) and

non-basal (4.49 Å, 2.57 Å, 1.70 Å, and 1, 50 Å) reflections with an indicative broad peak profile. In turn, quartz was identified by significantly sharper peaks at 3.34 Å, 4.28 Å, and 2.28 Å. Finally, anatase was identified by reflections 3.53 Å, 1.70 Å, and 1.67 Å. The high iron content in bentonite is most likely caused by isomorphic substitution in montmorillonites' octahedral sheets and also by its presence in accessory minerals.

Zeolite from the Sokernitskoye deposit for 71.8% is composed of clinoptilolite and admixture minerals such as quartz, illite, feldspar and a small amount of smectite. Zeolite (clinoptilolite) was identified by a series of main reflections: 11.94 Å, 9.02 Å, 7.94 Å, 6.79 Å, 6.65 Å, 5.25 Å, 5.13 Å, 3.97Å, 3.91 Å, etc. Quartz was identified by the sharp main peaks at 3.34 Å and 4.27 Å and a series of less intensive peaks in the large angles part of the pattern. Feldspar was identified by reflections in the range of 3.19–3.25 Å and a series of less intensive peaks. Smectite was detected by the analysis of X-ray diffraction patterns from oriented specimens in air-dry and ethylene glycol-solvated states.

Diatomite from the "BiaFa" company consists mainly of diatom shells with opal structure which makes up 80.8%. The sample also contained admixture minerals: 9.9% smectite, 9.0% kaolinite group minerals, and 0.3% quartz. As it was revealed by the FTIR data, the sample may also contain admixtures of sepiolite/pyrophyllite, however, it was not possible to quantify them using the XRD patterns from the raw sample without additional treatment. Smectite was identified by a series of reflections with the following spacing: 15.02 Å, 4.47 Å, 2.57 Å, 2.50 Å, and 1.51 Å. Minerals of the kaolinite group were identified by a series of peaks at 7.14 Å, 4.47 Å, and others. Quartz admixture was identified by one main sharp peak at 3.36 Å. A wide and intensive "halo" in the range of 18–30°2 indicates a high content of amorphous opal. Presence of aluminum, iron, calcium, and magnesium in the chemical composition of the sample is mainly due to the high content of smectite and kaolinite.

The IR-spectroscopy data were consistent with the mineral composition obtained by XRD. The FTIR spectra of the heated KBr-pellets are shown in Figure 2. The identification of minerals and absorption bands were performed in accordance with the recommendations of: Farmer [21] and Zviagina et al. [22] for glauconite; Madejova and Komadel [23,24] for bentonite; and Smith [25] and Guatame-Garcia and Buxton [26] for diatomite.

The studied sample of glauconite had all the characteristic features of the FTIR spectrum: a main band of Si-O stretching vibrations at 1000 cm^{-1}; and in the region of Si-O bending vibrations, there is a triplet of bands with the following positions: 495, 458 and 437 cm^{-1}. In the region of stretching vibrations of OH groups, there is a wide complex band at 3400–3700 cm^{-1}, which can be considered as a result of the superposition of individual absorption bands of the cation–OH–cation. There is an intense band at 3545 cm^{-1} (which corresponds to the superposition of the absorption bands of Fe^{2+}–OH–Fe^{2+}, Fe^{2+}–OH–Fe^{3+}, Fe^{3+}–OH–Fe^{3+}, Fe^{2+}–OH–Mg, Fe^{3+}–OH–Mg, and Al–OH–Fe^{2+}), a recognizable band at 3560 cm^{-1} (Al–OH–Fe^{3+}, and Mg–OH–Mg), and a minor band at ~3600 cm^{-1} (Al–OH–Mg and several Al–OH–Al bands). In addition to glauconite, trace amounts of impurities of silica (680 cm^{-1}) and carbonates (1404 cm^{-1} and 870 cm^{-1}) were noted.

The studied bentonite sample mainly consisted of Al-rich smectite. This is evidenced by the combination of the following characteristics of the IR spectrum: the most intense band of Si–O stretching is relatively symmetrical and located at 1043 cm^{-1}, with a doublet at 524 cm^{-1} (Al–O–Si deformation) and another at 467 cm^{-1} (Si–O–Si deformation); the absorption near 622 cm^{-1} corresponds to the coupled Al–O and Si–O out-of-plane vibrations, and the OH stretching and bending vibrations appear as the bands at 3634 and 918 cm^{-1}, respectively. Trace amounts of impurities of quartz (800 cm^{-1} and 780 cm^{-1}) and carbonates (1450 cm^{-1} and 880 cm^{-1}) were also noted.

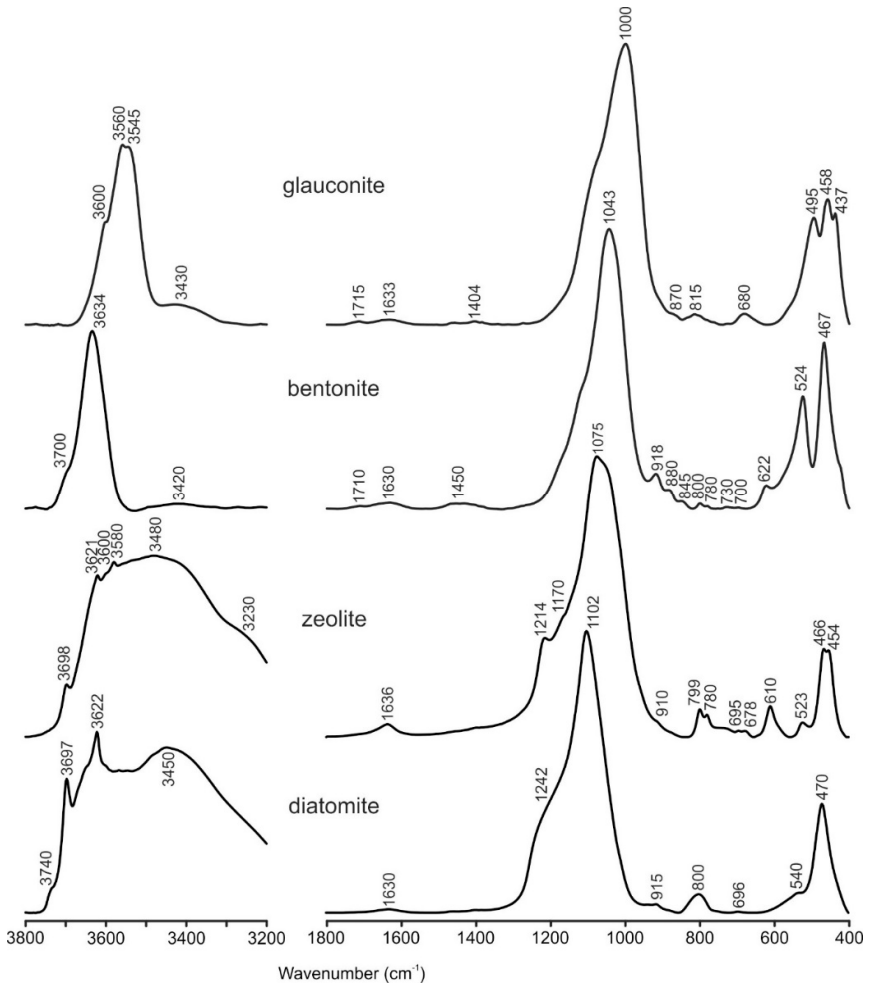

Figure 2. FTIR spectra of natural sorbents.

According to the XRD data, the diatomite sample mainly consists of opal-A$_N$, which is evidenced by a broad peak at 20–30°2θ CuK$_\alpha$. The IR-spectrum of the sample also shows some characteristics of opal bands: 1102 cm^{-1} caused by the asymmetric stretching of the [SiO_4] tetrahedron, 470 cm^{-1} associated with the Si–O–Si bending vibration mode; and a characteristic of diatoms: ~1240 cm^{-1} is due to free Si-OH molecular vibrations. In addition to opal, on the IR spectrum, the impurities of kaolinite (3697 cm^{-1}, 3622 cm^{-1}, and 915 cm^{-1}) and sepiolite/pyrophyllite (the appearance of a new weak band at 3740 cm^{-1} after heating, which is related to free (i.e., not bonded to water molecules) surface silanol groups, Si–OH) can be identified. Additionally, the presence of the smectite revealed by the XRD method could not be confidently identified by FTIR in this case because of the overlapping of the characteristic broad OH-stretching band at 3620–3630 cm^{-1} with the kaolinite bands.

The studied zeolite sample contains different zeolite minerals from the clinoptilolite-heulandite series and other admixtures. Therefore, due to the overlapping of bands from various minerals, it is impossible to obtain additional data on the mineral composition from the IR spectra.

SEM images of glauconite sample show clearly visible micro-aggregates with leaf-like shapes and a well-developed layer structure ranging in size from 0.5 to 2 μm, both in the form of individual particles and forming fine-grained aggregates up to the size of 110 μm in cross-section (Figure 3).

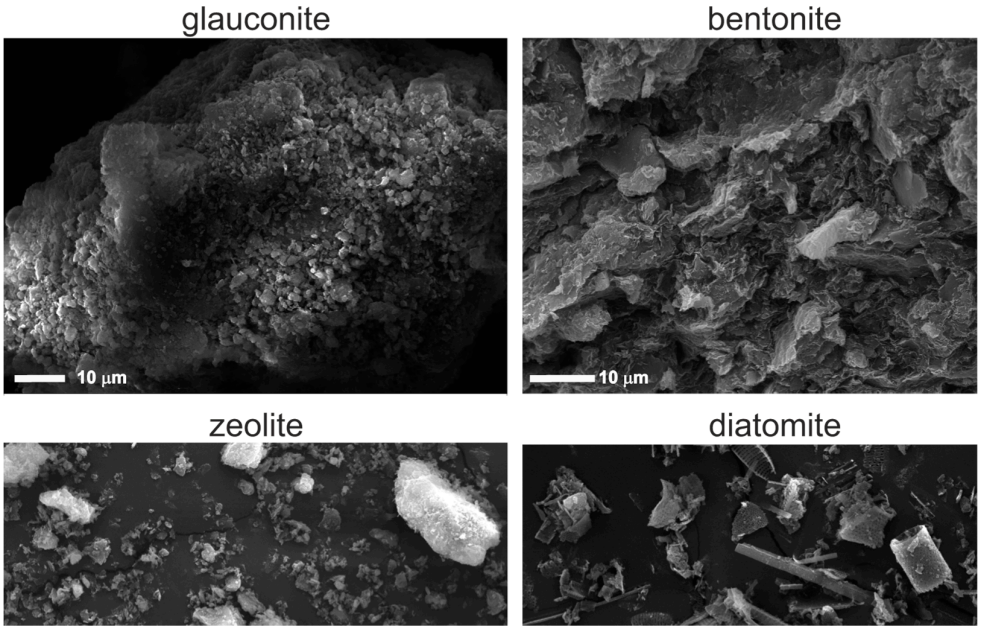

Figure 3. Scanning electron microscope images.

In the bentonite sample, montmorillonite particles are represented by thin leaf-shaped microaggregates with a diameter of 3–5 to 10–20 μm, which form a loose coarse-grained openwork microstructure. Contacts between particles occur as edge-to-edge and face-to-face configurations [27,28], resulting in the formation of very thin microaggregates.

SEM images of diatomite demonstrate the presence of different forms of diatom skeletons (frustules) with cylindrical particles, and also broken particles with pennate and acicular shapes with a well-developed porous structure. Cylindrical diatom skeletons are about 5–7 μm in diameter, and 8–10 μm in length. Diatom species are perforated by a differently shaped and sized network of pores: round pores (150–260 nm in diameter) and slit-shaped pores (450–860 nm in length).

Zeolite is represented by separate particles of leaf-like shape with size ranging from 0.3 to 1.5 μm and microaggregates with size ranging from 22 to 50 μm with the presence of dispersed particles of clay minerals on the surface (Figure 3).

3.2. Characterization of Specific Surface Area and Porosity

Data in Table 3 show that the specific surface area of all samples is quite small and mostly similar for bentonite, diatomite and glauconite. Moreover, the pore volume is two times smaller for glauconite and bentonite as compared with diatomite, which is associated with the presence of micropores (≈50% of total surface area).

The International Union of Theoretical and Applied Chemistry (IUPAC) recommended the following classification of pore sizes: macropores (>50 nm), mesopores (2–50 nm) and micropores (≤2 nm) [29–31]. The average measured pore size for all our samples was about 5 nm, which corresponds to interparticle pores, according to [32] or mesopores, according to the IUPAC.

Diagrams of pore size distribution are quite similar for zeolite and diatomite: the pore size ranges within 3–80 nm, the maximum number of pores is observed within the range of 3–15 nm (mesopores), while there is a small number of macropores (50–80 nm). Glauconite and bentonite differ by a pore size distribution shift towards smaller values: a range of 1.5–30 nm overall, a significant number of micropores with the size up to 2 nm and the absence of macropores.

Table 3. Textural properties of studied mineral sorbents.

Sample	Specific Surface Area SBET, m^2/g	Pores Volumecm^3/g, nm	Average Diameter, nm	Microporosity (Volume) (T-Method Halsey), cm^3/g	Specific Surface Area (T-method Halsey), SBET, m^2/g		
					Micropores	Meso-Macropores	Total
Glauconite	48	0.061	5.28	0.013	23	25	48
Bentonite	45	0.078	5.00	0.016	23	22	45
Zeolite	14	0.053	4.89	-	-	-	14
Diatomite	42	0.135	4.89	-	-	-	42

3.3. Cation Exchange Capacity

The problem of studying sorbents that differ greatly in mineral composition and properties (layered aluminosilicates, framework silicates, and silicites) is that there is no universal method for obtaining adequate data on CEC values. For example, the problems of CEC determining in zeolite samples using methylene blue have been repeatedly discussed in the literature [33]. For this purpose, for each sorbent, the most correct and widespread method for determining the CEC was selected, which, according to the authors, has important methodological significance.

CEC values determined by various methods are presented in Table 4. The measurement of zeolite's CEC by the method of exchange by NH_4^+ showed the highest value (161 meq/100 g), which is comparable with literature data on zeolites. The advantage of the ammonium chloride solution is its inability to form coordination complexes or sparingly soluble salts, as well as the selectivity of its adsorption by zeolite. The CEC values obtained using the method of exchange in BaCl2 solution (Mehlich's method) and MB are significantly lower: 17.6 and <3 meq/100 g, respectively. It is worth noting that the Mehlich's CEC should have given either comparable or slightly higher CEC values compared with the ammonium chloride method. Ba^{2+} have a higher replacing power, and its ionic radius varies from 1.49 to 1.75 Å depending on the coordination number, which is much smaller than the size of the zeolitic channels. However, the results indicate that barium did not replace the exchangeable cations in the zeolite channels, which is probably due to the use of a 0.1 M barium solution according to [14]. Very low CEC values determined by sorption of MB can be explained by the fact that methylene blue molecules are relatively large in size, approximately 1.25–1.6 nm in length, 0.57 nm in width and 0.84 nm in height [34]. Thus, so large molecules could not penetrate into the zeolite channels with a cross-section size of about 4.4–7.2 Å [33] and were sorbed on the surface of the mineral.

The obtained CEC values of glauconite using the Mehlich's method and MB adsorption are 12 and 17 meq/100 g, respectively. The obtained CEC values reveal the presence of a small number of smectitic interlayers, which are almost always present in the glauconite structure [35]. The adsorption of MB and most cations, including Cs, can occur on the surface of particles, in the interlayer space of smectite interlayers, and also on the illitic interlayer edge sites in wedge-shaped positions deficient of K^+ ions–the so-called frayed edge sites-FES [36].

The CEC values of bentonite according to MB turned out to be equal to 94 meq/100 g, which is quite typical for Na-bentonite and complies with published data [36,37]. The CEC values of diatomite determined with Mehlich's method and by adsorption of MB turned out to be quite close: 11.3 and 9.8 meq/100 g respectively. Since diatomite material consists of opal and does not have a negative charge associated with isomorphic substitutions in the mineral structure, the data obtained can be explained by the admixture of smectite and kaolinite-group minerals in the sample. Perhaps, in addition, dyes can be adsorbed on a well-developed surface of diatom frustules (SBET = 42 m^2/g) due to electrostatic interactions.

Table 4. Cation exchange capacity of the studied sorbents, meq/100 g.

	Adsorbate/Index Cation		
Sample	**Ba^{2+}**	**MB ($C_{16}H_{18}N_3S^+$)**	**NH_4^+**
Glauconite	12.2	16.6	
Bentonite		93.5	
Zeolite	17.6	<3	161.0
Diatomite	11.3	9.8	

3.4. Cesium Sorption

^{137}Cs sorption on the studied sorbents is shown in Figure 4. It is known that Cs is sorbed by the ion-exchange mechanism in a wide range of sorbents and conditions [38,39]. The main feature of this reaction is the independence of sorption from the pH values. Therefore, the sorption onto studied materials can also be described as an ion-exchange one. A number of studies have shown that sorption of cesium on bentonite [16], illite [40], zeolite [7] and diatomite [9] occurs quickly during the first hours of interaction. It has also been shown that the decrease in sorption observed at pH values below 4 can be explained by the competition between Cs^+ ions and H^+ [16,41]. The highest Kd values are obtained for samples of zeolite and glauconite (log K_d 4.0 and 3.8, respectively). Additionally, the effect of acidic conditions on smectite results in the partial release of interlayer and octahedral cations into solution [41]. The sample of Bentonite was chosen with a Na-form of montmorillonite. Exposure of acidic conditions at pH < 4 should lead to a partial exchange of interlayer Na^+ and the leaching of octahedral Al^{3+}, Mg^{2+} and $Fe^{2,3+}$ [41–43], which may further compete with Cs^+. At the same time, diatomite has a sufficient content of smectite and defective kaolinite (possibly halloysite or mixed mineral of the kaolinite-smectite range), which can also supply interlayer and octahedral cations in a solution at low pH, which in turn can compete with Cs^+. The potential partial destruction of the glauconite structure at low pH is much slower, which probably results in a less pronounced dependence of sorption rate on pH value.

Sorption values decrease as follows: zeolite ≥ glauconite > bentonite > diatomite (Table 5). High ^{137}Cs sorption on zeolite is explained by a quite large content of adsorption sites with high selectivity so that H^+ does not compete strongly with Cs^+ in acidic conditions and also with the size of the channels (4.4–7.2Å, as mentioned before). This suggests that a cesium ion with a diameter of 3.3A can fit into the intracrystalline channels. Thus, the zeolite structure, with its numerous adsorption sites, and suitable channel size provides good conditions for cesium sorption [44,45].

The relatively high sorption on glauconite (with a CEC of about 10 meq/100 g) laid the groundwork for a generalized cation exchange sorption model for the uptake of Cs by minerals of the illite group [40]. The model is based on the assumption of the existence of planar sorption centers (typical for most of the clay minerals) and also the existence of special FESs (frayed edge sites) formed by weathering of the clay particle's edges. It is possible to selectively replace the potassium with single-charged cations of low hydration energy and small radius–Cs^+, Rb^+, Li^+, or NH_4^+ in such damaged areas. A similar approach has been confirmed in subsequent studies [40,46,47]. Therefore, relatively high Cs sorption onto glauconite can be explained by high selectivity of its sorption sites towards this cation. The higher Cs sorption can also be explained by the higher charge of glauconite layer and its localization in tetrahedral sheets.

Currently, there is no consensus in the literature regarding the mechanism of interaction of Cs with clay minerals. A number of authors provide evidence for the occurrence of exclusively ionic reactions [47–51], some studies indicate the formation of inter- and outer-sphere conplexes of cesium with edge centers and interlayer space [39,52,53]. The spectral methods [52,53] make it possible to detect complexes at high concentrations of cesium, but cannot be used at concentrations of Cs = 10^{-6} M. The pH dependence observed in this work can be explained both by the formation of inner- and outer-sphere complexes, and by competition with leached cations, or it could be a consequence of both processes.

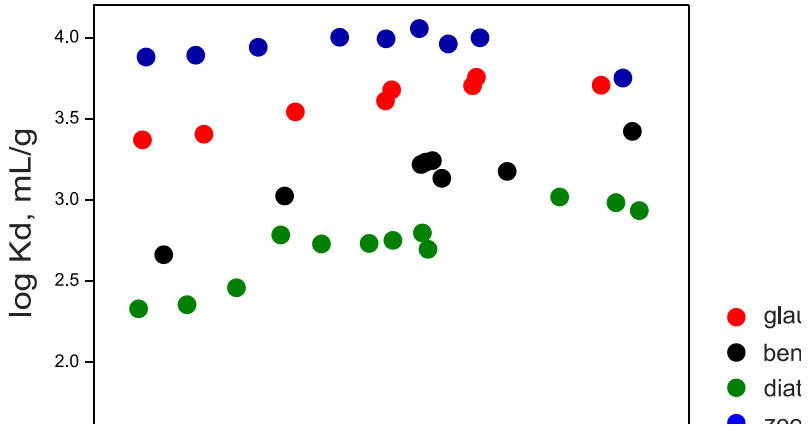

Figure 4. pH-dependence of ^{137}Cs sorption onto the studied sorbents ((^{137}Cs) = 10^{-6} M, (solid phase) = 1 g/L, ionic strength = 0.01 M $NaClO_4$).

The rate of ^{137}Cs sorption on bentonite is slightly lower than that on glauconite, due to the lower affinity of montmorillonite sorption sites. Cs is predominantly sorbed in planar sites on the external surface and in the interlayer. The nature of these centers is similar in the case of illites and smectites [54,55], but the impact of FES on cesium adsorption on montmorillonite is probably less important. Literature data for this vary: 0.55 μmol/g [50], 0.5 μmol/g [47], 0.462 μmol/g [49], 0.592 μmol/g [48]. Considering that in our experiments the content of glauconite was 1 g/L, the FES concentration according to published data is in the range of 5×10^{-7} M, which is comparable with the used Cs concentration of 10^{-6} M. It is worth noting that in acidic conditions glauconite shows a slight dependency of sorption on pH (Figure 4), probably because of the presence of smectitic interlayers which is quite usual for illites and glauconites [35] and the mechanism of this dependency is the same as described above for bentonite.

Lower values of ^{137}Cs sorption on diatomite are related to a principally different structure. In this case, binding may occur with silanol (≡SiOH) groups [52]. However, in this case, impurities of smectite and kaolinite in the diatomite sample make the most significant impact on cesium adsorption onto diatomite material. It also should be noted that the adsorption experiment described in the article [56] was carried out on a rock sample with a high content of clay minerals, at least 30% based on the X-ray diffraction picture presented in the work. Moreover, the reflection in the region of 10 Å was erroneously referred to as muscovite instead of mixed-layer minerals of the illite-smectite series.

Table 5. K_d values for ^{137}Cs sorption onto the studied sorbents at pH = 7.0 ± 0.2 in 0.01M $NaClO_4$ solution.

Sorbent	log K_d, mL/g
Glauconite	3.6
Bentonite	2.8
Zeolite	4.0
Diatomite	2.7

Studies of the reversibility of cesium sorption showed (Figure 5) that the values of desorption increase in the following series: zeolite < bentonite ~ diatomite < glauconite. Thus, it can be assumed that cesium is irreversibly bound in the channels of the zeolite (desorption was less than 3%). In the case of montmorillonite and montmorillonite-dominated clays, sorption is believed to be reversible [48,57,58], however recent works have shown that some fixation of intrinsic Cs may be achieved by the addition of divalent cations before desorption [59,60].

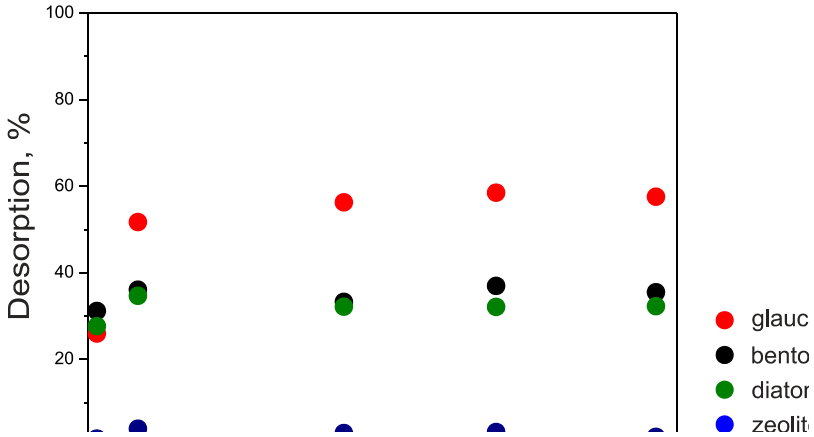

Figure 5. Kinetics of cesium desorption from samples with a model solution ($NaHCO_3$—96.0 mg/L, $CaSO_4 2H_2O$—60.0 mg/L,$MgSO_4$—60.0 mg/L, KCl—4.0 mg/L).

The proximity of the desorption values on the diatomite and bentonite samples can indicate the dominant role that montmorillonite plays in cesium sorption for these samples. On a glauconite sample, undesorbed cesium is apparently firmly fixed with FES, as described in [48,61]. The binding of cesium not only to FES, but also with other types of sorption centers causes a high degree of desorption.

4. Conclusions

This research made it possible to reveal the principal factors affecting efficiency and mechanisms of ^{137}Cs sorption on natural sorbents. Together with the global parameters, such as CEC and specific surface area, the presence of argillaceous minerals and their structural features are among the most important factors. Therefore, detailed mineralogical studies were required for the interpretation of the results of sorption experiments on natural sorbents, and in the design of their real-life application.

The highest cesium sorption value was observed on zeolite, due to its high CEC (161 mg eq/100 g). Cesium sorption on zeolite occurs mainly through the ion-exchange reaction. The higher sorption value on glauconite in comparison with bentonite is primarily caused by the high layer charge which is mainly localized in tetrahedral sheets and also with the existence of highly selective sorption centers (Frayed Edge Sites) on the glauconite surface, and competition with interlayer sodium in montmorillonite, especially at low pH values. Despite the fact that the main mechanism for sorption of cesium is ion exchange, the CEC of the minerals was not the main determining factor of sorption. For example, glauconite, which has a relatively low CEC, shows one of the highest results, ahead of bentonite, which is associated with its structural features.

Cesium sorption on diatomite is mostly provided by the presence of smectite and kaolinite in the sample composition. Non-typical pH-dependent cesium sorption is caused by competition with Na^+ cations, and possibly octahedral Al^{3+}, Mg^{2+}, and $Fe^{2,3+}$ leached from the mineral structure at low pH. Since the physical adsorption of cesium on the surface of minerals plays the smallest role, there is no clear connection between the sorption value and the specific surface area, which is especially clearly seen in the case of diatomite.

Desorption experiments showed a practically irreversible bond of cesium in the zeolite sample (desorption less than 3%). The binding of cesium in bentonite, diatomite and glauconite is not completely reversible and is associated with Cs interaction with various sorption centers. The obtained results will help in the consideration and choice of minerals used as promising sorbents.

Author Contributions: Petr Belousov: prepared material, conceived design of the experiments and wrote the paper; Anna Semenkova and Tatiana Egorova: carried out sorption experiments with radionuclides; Sergey Zakusin: carried out X-ray diffraction analysis; Olga Dorzhieva: carried out infrared spectroscopy (FT-IR) analysis; Ekaterina Tyupina: analyzed specific surface area and porosity; Inna Tolpeshta, Yulia Izosimova:

carried out CEC determination; Michail Chernov: studied samples by scanning electron microscopy; Victoria Krupskaya: collected the data for mineral analysis and interpretation.

Funding: The study was supported by the Russian Science Foundation, project no. 18-77-00015 (zeolite, diatomite, glauconite) and the Grant of the Russian Foundation for Basic Research no. 18-29-12115 (bentonite study).

Acknowledgments: Micromorphology (SEM) was studied in the frame of the IGEM RAS base theme № AAAA-A18-118021590167-1. Experimental studies were partially performed using the equipment acquired with the funding of Moscow State University Development Program (X-ray Diffractometer Ultima-IV, Rigaku and Scanning Electron Microscope LEO 1450VP, Carl Zeiss).

Conflicts of Interest: The authors declare no conflict of interest. The study was supported by the Russian Science Foundation, project no. 18-77-00015 and the Grant of Russian Foundation for Basic Research no. 18-29-12115. The founding sponsors had no role in the design of the study; in the collection, analyses, or interpretation of the data; in the writing of the manuscript; or in the decision to publish the results.

References

1. Bergaya, F.; Theng, B.K.G.; Lagaly, G. *Handbook of Clay Science;* Elsevier: Amsterdam, The Netherlands, 2006; Volume 1, p.1246.
2. Grauer, R. Bentonite as a backfill material in a high- level waste repository. *MRS Bull.* **1994**, *19*, 43–46.
3. Sellin, P.; Olivier, X. Leupin. The Use of Clay as an Engineered Barrier in Radioactive-Waste Management—A Review. *Clays Clay Miner*. **2013**, *61*, 477–498.
4. Guggenheim, S.; Adams, J.M.; Bain, D.C.; Bergaya, F.; Brigatti, M.F.; Drits, V.A.; Formoso, M.L.L.; Galan, E.; Kogure, T.; Stanjek, H. Summary of recommendations of Nomenclature Committees relevant to clay mineralogy: Report of the Association Internationale Pour L'etude des Argiles (AIPEA) nomenclature committee for 2006. *Clays Clay Miner.* **2006**, *54*, 761–772.
5. Osmanlioglu, A.E. Natural diatomite process for removal of radioactivity from liquid waste. *Appl. Radiat. Isot.* **2007**, *65*, 17–20.
6. Taylor, P.; Mimura, H.; Kanno, T. Distribution and Fixation of Cesium and Strontium in Zeolite A and Chabazite. *J. Nucl. Sci. Technol.* **1985**, *22*, 284–291.
7. El-Kamash, A.M. Evaluation of zeolite A for the sorptive removal of $Cs^{+}$and Sr^{2+} ions from aqueous solutions using batch and fixed bed column operations. *J. Hazard. Mater.* **2008**, *151*, 432–445.
8. Borai, E.H.; Harjula, R.; Malinen, L.; Paajanen, A. Efficient removal of cesium from low-level radioactive liquid waste using natural and impregnated zeolite minerals. *J. Hazard. Mater.* **2009**, *172*, 416–422.
9. Nenadović, S.; Kljajević, L.; Marković, S.; Omerašević, M.; Jovanović, U.; Andrić, V.; Vukanac, I. Natural diatomite (Rudovci, Serbia) as adsorbent for removal Cs from radioactive waste liquids. *Sci. Sinter.* **2015**, *47*, 299–309.
10. Moore, D.M.; Reynolds, R.C., Jr. *X-ray Diffraction and the Identification and Analysis of Clay Minerals*, 2nd ed.; Oxford University Press: Oxford, UK; New York, NY, USA, 1999; p. 378.
11. Post, J.E.; Bish, D.L. Rietveld refinement of crystal structures using powder X-ray diffraction data. *Rev. Miner. Geochem.* **1989**, *20*, 277–308.
12. Doebelin, N.; Kleeberg, R. Profex: A graphical user interface for the Rietveld refinement program BGMN. *J. Appl. Cryst.* **2015**, *48*, 1573–1580.
13. Cokca, E.; Birand, A. Determination of Cation Exchange Capacity of Clayey Soils by the Methylene Blue Test. *Geotech. Test. J.* **1993**, *16*, 518–524.
14. Alexander, E.B. Cation-exchange capacity of acid soils Using aluminum chloride and barium chloride-trietha nolamine. soil sci. *Soc. Am. J.* **1976**, *40*, 961–963.
15. Tucker, B.M. Laboratory Procedures for Cation Exchange Measurement on Soils. Available online: https://trid.trb.org/view/37268 (accessed on 10 October 2019)
16. Semenkova, A.S.; Evsiunina, M.V.; Verma, P.K.; Mohapatra, P.K.; Petrov, V.G.; Seregina, I.F.; Bolshov, M.A.; Krupskaya, V.V.; Romanchuk, A.Y.; Kalmykov, S.N. Cs^{+} sorption onto Kutch clays: Influence of competing ions. *Appl. Clay Sci.* **2018**, *166*, 88–93.
17. Goldberg S.; Criscenti L. J.; Turner D. R.; Davis J. A.; Cantrell K. J. Adsorption–Desorption Processes in Subsurface Reactive Transport Modeling. *Vadose Zone J.* **2007**, *6(3)*, 407–435.

18. Payne T.E.; Brendler V.; Ochs M.; Baeyens B.; Brown P.L.; Davis J.A.; Ekberg C.; Kulik D.A.; Lutzenkirchen J.; Missana T.; Tachi Y.; Van Loon L.R.; Altmann S. Guidelines for thermodynamic sorption modelling in the context of radioactive waste disposal. *Environ. Model. Softw.* **2013**, *42*, 143–156.
19. Geckeis H.; Lützenkirchen J.; Polly R.; Rabung T.; Schmidt M. Mineral–Water Interface Reactions of Actinides. *Chem. Rev.* **2013**, *113*, 1016–1062.
20. *Short-Term Methods for Estimating the Chronic Toxicity of Effluents and Receiving Waters to Marine and Estuarine Organisms*, 2nd ed.; U.S. Environmental Protection Agency: Washington, DC, USA, 2002; p. 486.
21. Farmer, V.C. *The Infrared Spectra of Minerals*; Monograph 4, Book Section 16; Mineralogical Society: London, UK, 1974; p. 539.
22. Zviagina, B.B.; Drits, V.A.; Sakharov, B.A.; Ivanovskaya, T.A.; Dorzhieva, O.V.; McCarty, D.K. Crystal-chemical regularities and identification criteria in Fe-bearing K-dioctahedral micas 1M from X-ray diffraction and Infrared spectroscopy data. *Clays Clay Miner.* **2017**, *65*, 234–251.
23. Madejovà, J.; Komadel, P. Baseline studies of The Clay Minerals Society source. Clays: Infrared Methods. *Clays Clay Miner.* **2001**, *49*, 410–432.
24. Madejovà, J.; Komadel, P. Information available from infrared spectra of the fine fractions of bentonites. In *The Application of Vibrational Spectroscopy to Clay Minerals and Layered Double Hydroxides*; CMS Workshop Lectures; The Clay Mineral Society: Aurora, CO, USA, 2005; Volume 13, pp. 65–98.
25. Smith, D.K. Opal, cristobalite, and tridymite: Noncrystallinity versus crystallinity, nomenclature of the silica minerals and bibliography. *Powder Diffr.* **1998**, *13*, 2–19.
26. Guatame-Garcia, A.; Buxton, M. The Use of Infrared Spectroscopy to Determine the Quality of Carbonate-Rich Diatomite Ores. *Minerals* **2018**, *8*, 53–66.
27. Van Olphen, H. *An Introduction to Clay Colloid Chemistry*; Wiley-Interscience: New York, NY, USA, 1963; p. 301.
28. Lagaly, G.; Ziesmer, S. Colloid chemistry of clay minerals: The coagulation of montmorillonite dispersions. *Adv. Colloid Interface Sci.* **2003**, *100–102*, 105–128.
29. IUPAC. Manual of Symbols and Terminology. *Pure Appl. Chem.* **1972**, *31*, 577.
30. Rouquerolt, J.; Avnir, D.; Fairbridge, C.W.; Everett, D.H.; Haynes, J.H.; Pernicone, N.; Ramsay, J.D.F.; Sing, K.S.W.; Unger, K.K. Recommendations for the characterization of 830 porous solids. *Pure Appl. Chem.* **1997**, *66*, 1739–1758.
31. Karnauhov, A.P. Adsorption. In *Texture of Dispersive and Porous Materials*; Nauka: Novosibirsk, Russia, 1999; p. 470. (In Russian)
32. Osipov, V.I.; Sokolov, V.N. Clays and their properties. In *Composition, Structure and Formation of Properties*; GEOS: Moscow, Russia, 2013; p. 576.
33. Haggerty, G.M.; Bowman, R.S. Sorption of chromate and other inorganic anions by organo-zeolite. *Environ. Sci. Technol.* **1994**, *28*, 452–458.
34. Mansouri, N.; Rikhtegar, N.; Panahi, H.; Atabi, F.; Karimi, S.B. Porosity, characterization and structural properties of natural zeolite—clinoptilolite—as a sorbent. *Environ. Prot. Eng.* **2013**, *39*, 139.
35. Ivanovskaya, T.A.; Zvyagina, B.B.; Sakharov, B.A.; Zaitseva, T.S. Crystal-chemical peculiarities of globular layer silicates of the glauconite-illite composition (Upper Proterozoic, Northern Siberia). *Lithol. Miner. Resour.* **2012**, *47*, 491–512.
36. Zaunbrecher, K.L.; Cygan, R.; Elliott, W.C. Molecular Models of Cesium and Rubidium Adsorption on Weathered Micaceous Minerals. *J. Phys. Chem. A* **2015**, *119*, 5691–5700.
37. Dohrmann, R.; Genske, D.; Karnland, O.; Kaufhold, S. Interlaboratory CEC and exchangeable cation study of bentonite buffer materials: I. Cu(II)-triethylenetetramine method. *Clays Clay Miner.* **2012**, *60*, 162–175.
38. Lieser K.H.; Steinkopff, T. Chemistry of Radioactive Cesium in the Hydrosphere and in the Geosphere. *Radiochim. Acta* **1989**, *46*, 39–47.
39. Wissocq, A.; Beaucaire, C.; Latrille, C. Application of the multi-site ion exchanger model to the sorption of Sr and Cs on natural clayey sandstone. *Appl. Geochem.* **2018**, *1*, 11.
40. Comans, N.J.; Haller, R.; De Preter, M.P. Sorption of cesium on illite: Non-equilibrium behaviour and reversibility. *Geochim. Cosmochim. Acta* **1991**, *55*, 433–440.
41. Krupskaya, V.; Zakusin, S.; Tyupina, E.; Dorzhieva, O.; Zhukhlistov, A.; Belousov, P.; Timofeeva, M. Experimental Study of Montmorillonite Structure and Transformation of Its Properties under Treatment with Inorganic Acid Solutions. *Minerals* **2017**, *7*, 49.

42. Krupskaya, V.V.; Zakusin, S.V.; Tyupina, E.A.; Dorzhieva, O.V. Transformation of Structure and Adsorption Properties of Montmorillonite under Thermochemical Treatment. *Geochem. Int.* **2019**, *57*, 314–330.
43. Krupskaya, V.; Novikova, L.; Tyupina, E.; Belousov, P.; Dorzhieva, O.; Zakusin, S.; Kim, K.; Roessner, F.; Badetti, E.; Brunelli, A.; et al. The influence of acid modification on the structure of montmorillonites and surface properties of bentonites. *Appl. Clay Sci.* **2019**, *172*, 1–10.
44. Puigdomenech, I. Make Equilibrium Diagrams Using Sophisticated Algorithms (MEDUSA). In *Inorganic Chemistry;* Royal Institute of Technology: Stockholm, Sweden, 2004.
45. Song, K.C.; Lee, H.K.; Moon, H.; Lee, K.J. Simultaneous removal of the radiotoxic nuclides Cs-137 and I-129 from aqueous solution. *Sep. Purif. Technol.* **1997**, *12*, 215–227.
46. Englehardt, D. Original Contribution Pozzolanic Filtration/Solidification of Radionuclides in Nuclear Reactor Cooling Water. *Waste Manag.* **1996**, *15*, 585–592.
47. Bradbury, M.H.; Baeyens, B.A. Generalised sorption model for the concentration dependent uptake of **caesium** by argillaceous rocks. *J. Contam. Hydrol.* **2000**, *42*, 141–163.
48. Durrant, C.B.; Begg, J.D.; Kersting, A.B.; Zavarin, M. Cesium sorption reversibility and kinetics on illite, montmorillonite, and kaolinite. *Sci. Total Environ.* **2018**, *610–611*, 511–520.
49. Missana, T.; García-Gutiérrez, M.; Benedicto, A.; Ayora, C.; De-Pourcq, K. Modelling of Cs sorption in natural mixed-clays and the effects of ion competition. *Appl. Geochem.* **2014**, *49*, 95–102.
50. Poinssot, C.; Baeyens, B.; Bradbury, M.H. Experimental and modeling studies of caesium sorption on illite. *Clays Clay Miner.* **1999**, *63*, 3217–3227.
51. Tachi, Y.; Yotsuji, K.; Seida, Y.; Yui, M. Diffusion and sorption of Cs^+, I^-, and HTO in samples of the argillaceous Wakkanai formation from the Horonobe URL, Japan: Clay-based modeling approach. *Geochem. Cosmochim. Acta* **2011**, *75*, 6742–6759.
52. Bostick, B.; Vairavamurthy, M.; Karthikeyan, K.; Chorover, J. Cesium Adsorption on Clay Minerals: An EXAFS Spectroscopic Investigation. *Environ. Sci. Technol.* **2002**, *36*, 2670–2676.
53. Yamaguchi, A.; Tanaka, M.; Kurihara, Y.; Takahashi, Y. Local structure of strontium adsorbed on 2:1 clay minerals and itscomparison with cesium by XAFS in terms of migration of theirradioisotopes in the environment. *J. Radioanal. Nucl. Chem.* **2018**, *17*, 545–551.
54. Kalinichev, A.G.; Loganathan, N.; Wakou, B.F.N.; Chen, Z. Interaction of ions with hydrated clay surfaces: Computational molecular modeling for nuclear waste disposal applications. *Proc. Earth Planet. Sci.* **2017**, *17*, 566–569.
55. Loganathan, N.; Kalinichev, A.G. Quantifying the Mechanisms of Site-Specific Ion Exchange at an Inhomogeneously Charged Surface: Case of Cs^+/K^+ on Hydrated Muscovite Mica. *J. Phys. Chem.* **2017**, *121*, 7829–7836.
56. Jovanovic, U.; Vukanac, I.; Kljajevic, L.; Nenadovic, S.; Andric, V.; Omerasevic, M.; Markovic, S. Natural diatomite (Rudovci, Serbia) as adsorbent for removal Cs from radioactive waste liquids. *Sci. Sinter.* **2016**, *47*, 299–309.
57. Iijima, K.; Tomura, T.; Shoji, Y. Reversibility and modeling of adsorption behavior of cesium ions on colloidal montmorillonite particles. *Appl. Clay Sci.* **2010**, *49*, 262–268.
58. Missana, T.; García-Gutiérrez, M.; Alonso, Ú.; Kinetics and irreversibility of cesium and uranium sorption onto bentonite colloids in a deep granitic environment. *Appl. Clay Sci.* **2004**, *26*, 137–150.
59. Fukushi, K.; Sakai, H.; Itono, T.; Tamura, A.; Arai, S. Desorption of intrinsic cesium from smectite: Inhibitive effects of clay particle organization on cesium desorption. *Environ. Sci. Technol.* **2014**, *48*, 10743–10749.
60. Fukushi, K.; Fukiage, T. Prediction of Intrinsic Cesium Desorption from Na-Smectite in Mixed Cation Solutions. *Environ. Sci. Technol.* **2015**, *49*, 17.
61. Nakao, A.; Thiry, Y.; Funakawa, S.; Kosaki, T. Characterization of the frayed edge site of micaceous minerals in soil clays influenced by different pedogenetic conditions in Japan and northern Thailand. *Soil Sci. Plant Nutr.* **2008**, *54*, 479–489.